Vol 15 No 12, December 2006
1009-1963/2006/15(12)/2942-05
Chinese Physics
© 2006 Chin. Phys. Soc.
and IOP Publishing Ltd

Hanbury-Brown and Twiss type double-slit interference with photorefractive fanning light*

Xiong Jun(熊 俊), Li Hong-Guo(李洪国), Sun Xu-Juan(孙绪娟),
Lin Lu-Fang(林露芳), and Wang Kai-Ge(汪凯戈)†

Department of Physics, Applied Optics Beijing Area Major Laboratory,
Beijing Normal University, Beijing 100875, *China*

(Received 24 January 2006; revised manuscript received 21 June 2006)

This paper reports that when an intense extraordinary-polarized laser beam illuminates a photorefractive $BaTiO_3$ crystal, the dynamic beam fanning light is formed to be a thermal-like light source with a long correlation time and wide spectral bandwidth. The experimental results of the first- and second-order double-slit interference with such photorefractive fanning light source, can be understood with the theoretical simulation in terms of Hanbury-Brown and Twiss effect.

Keywords: subwavelength interference, thermal light, photorefractive beam fanning, Hanbury-Brown and Twiss effect
PACC: 4225H, 4250, 7820W

1. Introduction

In a common viewpoint, interference is related to the coherence of optical field, and the disorder of a light source may destroy the interference fringes. But this is not true for high-order interference. Recent theoretical and experimental studies show that a thermal light source can perform high-order double-slit interference,[1−5] exhibiting subwavelength interference characteristics, which is similar to the results of entangled photon pair generated in the spontaneous parametric down-conversion.[6] Thermal light can also be used in ghost imaging.[7−14]

The thermal light sources used in experiments can be either pseudo- or true ones. In Refs.[4,11,12], the authors use a pseudo-thermal light source which is available by passing a laser beam through a slowly rotating ground glass disc. In the following works shown in Refs.[5,14], a true thermal light source, such as a commercial rubidium hollow-cathode lamp which emits chaotic light by atomic spontaneous emission, is applied. To show a subwavelength interference pattern, the thermal light must have a wide spectral bandwidth.[1] However, in order to detect the dynamic thermal fluctuation in the experimental observation, the response time of the detectors must be less than the correlation time of the light. The pseudo-thermal source has a longer correlation time since the ground glass rotates slowly and is illuminated by a monochromatic laser beam. Nevertheless, the correlation time of the true thermal light is the decay time of the atomic spontaneous emission of the order of a nanosecond. Therefore, for the pseudo-thermal light source, one may use detectors with longer response time than that for the true thermal light source. If the response time of detectors is not short enough with respect to the correlation time of light, the visibility of the interference fringe will be degraded. This could be one of the reasons that the visibility of fringe for the pseudo-thermal light experiment in Ref.[4] is much better than that for the true thermal light in Ref.[5].

In this paper, we report the experimental observation of the second-order double-slit interference with a dynamic photorefractive fanning beam, an incoherent light source exhibiting thermal statistics. Beam fanning is a basic phenomenon in photorefractive crystals. In some cases, beam fanning is undesirable. But it is an important factor in the operation of self-pumped phase conjugation. Various studies of the mechanism of beam fanning have been reported.[15−21] Feinberg proposed a self-defocusing mechanism for fanning effect in which the Gaussian shape of the beam causes

*Project supported by the National Fundamental Research Program of China (Project No 2001CB309310), and the National Natural Science Foundation of China (Project No 10574015).
†Corresponding author. E-mail: wangkg@bnu.edu.cn

the fan.[15] Another mechanism is that the beam fanning is the amplification of the scattered noise by two-beam coupling.[16−21] In general, the intensity distribution of beam fanning is stable after a transient period according to the above theory. However, Xiong *et al* observed a dynamic intensity distribution of beam fanning when an intense laser beam illuminated a $BaTiO_3$ crystal, showing that the intensity of each pixel in such dynamic beam fanning was fluctuating in time.[22] In the present experiment, we observe the first- and second-order double-slit interference patterns by measuring the intensity distribution and the joint-intensity distribution of the dynamic fanning light in the detection plane. The experimental results show that the dynamic photorefractive beam fanning is a better thermal-like light source, which can perform the second-order double-slit interference pattern, in agreement with the theoretical predictions.

2. Experiment

The experimental setup is shown in Fig.1.

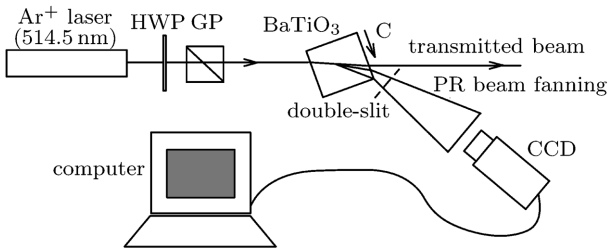


Fig.1. Sketch of the experimental setup. HWP represents the half wave plate, and GP the Glan–Taylor polarizer.

An CW Argon ion laser of wavelength 514.5 nm is used to illuminate a 6 mm × 6 mm × 6 mm photorefractive $BaTiO_3$ crystal. The combination of a half wave plate (HWP) and a Glan-Taylor polarizer (GP) is placed between laser and $BaTiO_3$ crystal for changing incident intensity and guaranteeing extraordinary-polarized beam incidence onto crystal. A dynamic beam fanning which has a time-dependent speckle pattern is produced when an intense e-polarized laser beam (e.g.185 mW) propagates through the photorefractive $BaTiO_3$ crystal. Figure 2 shows the speckle pattern in the beam fanning grabbed with a Mintron 1881 EX CCD camera, which has a frame format of 795 × 596 pixels with pixel size of 8.6 μm × 8.3 μm, and Fig.3 shows a typical intensity fluctuation of a pixel in the beam fanning.

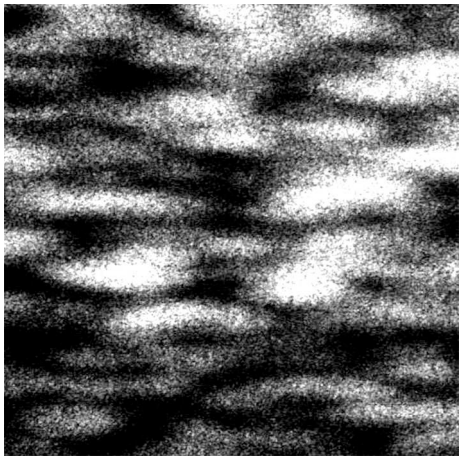


Fig.2. Enlargement of spatial distribution of the beam fanning from $BaTiO_3$ crystal. The picture of dimension of 7mm×7mm was taken from the screen 515mm away from $BaTiO_3$ crystal.

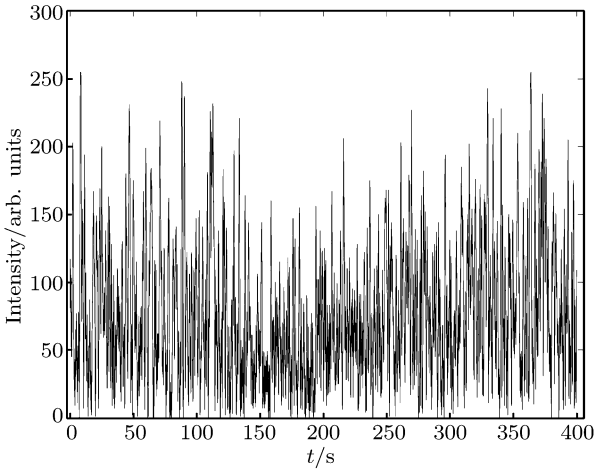


Fig.3. Intensity fluctuation of a pixel in beam fanning from $BaTiO_3$ crystal.

The correlation time τ_{coh} of the fanning beam is measured to be about 850 ms. Then we perform Young's double-slit interference experiment where the double-slit is placed at a distance of 5 mm from the crystal. The two slits are separated by $d = 100\,\mu$m and have a width $b = 55\,\mu$m. The diffracted radiation is recorded with the CCD camera, located at a distance of 510 mm from the double-slit. The grey values of all 795 pixels in a horizontal line are registered in 0.67 ms which is much shorter than the correlation time τ_{coh}. The frames are grabbed at a rate of 25 Hz. By evaluating the average of the product of any two pixels over a 400 seconds interval, we obtain the joint-intensity correlation $\langle I_1(x_1)I_2(x_2)\rangle$, where $I_1(x_1)$ and $I_2(x_2)$ are the light intensities detected by pixel 1 and pixel 2 at the positions x_1 and x_2 respectively. For comparison, we also measured the first-order interference pattern of the coherent light of wavelength of 514.5 nm by us-

ing the same experimental setup. The experimental results are plotted in Figs.4, 5.

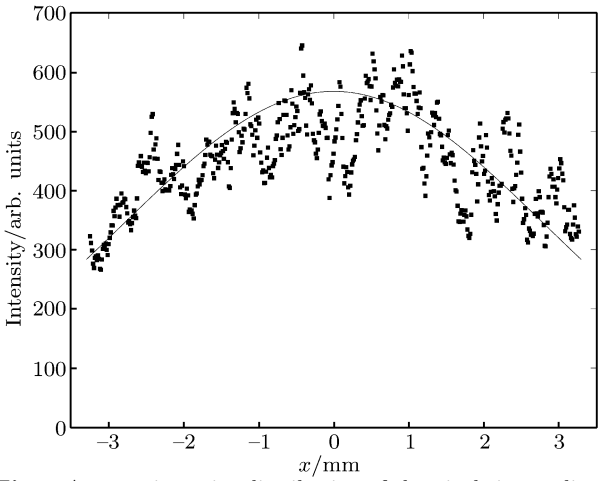


Fig.4. Average intensity distribution of the pixels in one line in CCD camera. The solid line represents the numerical simulation.

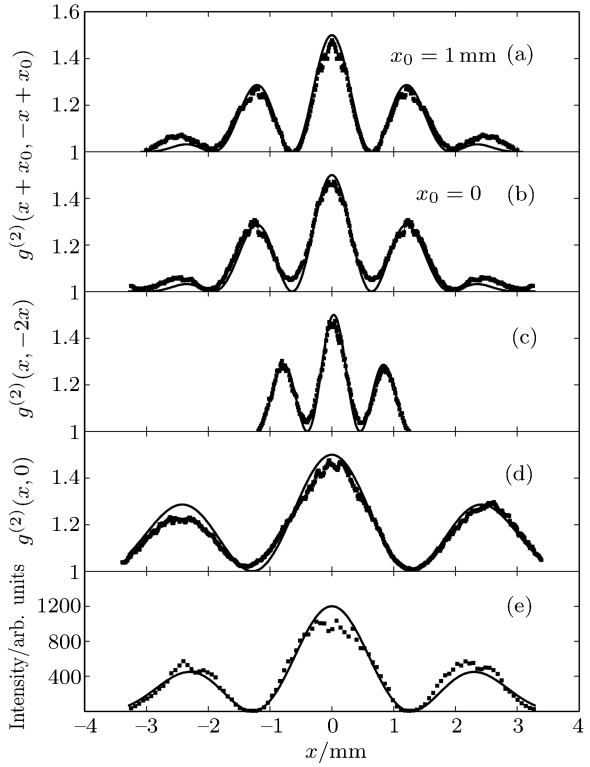


Fig.5. The interference patterns obtained by measuring the normalized joint-intensity correlation function, (a) $g^{(2)}(x + x_0, -x + x_0)$, where $x_0 = 1$ mm, (b) $g^{(2)}(x + x_0, -x + x_0)$, where $x_0 = 0$ mm, (c) $g^{(2)}(x, -2x)$, and (d) $g^{(2)}(x, 0)$. For comparison, (e) shows the first-order intensity distribution for coherent light. The solid lines represent the numerical simulations.

In Fig.4, the intensity distribution is measured by scanning the single pixel. It can be seen that the incoherent beam fanning produces a diffraction pattern without fringes. From Fig.5(a) through Fig.5(d), we evaluate the normalized joint-intensity correlation $g^{(2)}(x_1, x_2) = \langle I_1(x_1)I_2(x_2)\rangle/[\langle I_1(x_1)\rangle\langle I_2(x_2)\rangle]$ for the fanning thermal-like beam according to the registered data by the CCD camera. For the sake of comparison, the measured first-order interference pattern for the coherent light with the same wavelength is plotted in Fig.5(e). Figures 5(a) and 5(b) are the interference patterns $g^{(2)}(x + x_0, -x + x_0)$ for two different symmetric centres $x_0 = 1$ and 0 mm respectively, where $x_0 = 0$ is the symmetric centre of the double-slit setup. Both patterns show the same subwavelength characteristic with respect to the first-order interference pattern of the laser beam, as shown in Fig.5(e). Furthermore, in Fig.5(c), we plot the correlation function $g^{(2)}(x, -2x)$ which shows the fringe interval narrower by a factor of 3 than that of the first order interference for the coherent light. In Fig.5(d), we show the correlation $g^{(2)}(x, 0)$, i.e. by fixing one pixel at the symmetric centre and scanning the pixel along x, the same pattern as the first-order interference for the coherent beam is obtained. The visibilities of these second-order interference patterns for the incoherent beam fanning are about 20%.

3. Theoretical description

The theoretical explanation of the second-order interference for the thermal light has been illustrated in Refs.[1,4]. In the interference plane, the first order correlation is written as[4]

$$G^{(1)}(x_1, x_2) = C_1 \int \widetilde{T}(\frac{kx_1}{R} - q)\widetilde{T}(\frac{kx_2}{R} - q)S(q)\mathrm{d}q, \tag{1}$$

where $S(q)$ is the spatial frequency spectrum of the thermal light, R is the distance between the double-slit and the detection plane, $k = 2\pi/\lambda$ is the wave number, and C_1 is a constant. Function $\widetilde{T}$ is the Fourier transform of the double-slit function given by $\widetilde{T}(q) = (2b/\sqrt{2\pi})\mathrm{sinc}(qb/2)\cos(qd/2)$. We assume that the beam fanning has a Gaussian type spectrum $S(q) = (\sqrt{2\pi}w)^{-1}\exp[-q^2/(2w^2)]$, where w is the bandwidth of spatial frequency. For better fitting to the experimental data in Fig.4, $wb/(2\pi)$ is taken as 0.446.

The second-order interference pattern is described as

$$g^{(2)}(x_1, x_2) = 1 + C_2 \times \mathrm{sinc}^2\left[\frac{\pi b(x_1 - x_2)}{\lambda R}\right] \cos^2\left[\frac{\pi d(x_1 - x_2)}{\lambda R}\right], \tag{2}$$

where C_2 describes the deviation from perfect thermal correlation. For ideal thermal correlation, $C_2 = 1$, and the maximum value of the normalized second-order correlation is 2. However, the experimental data of the interference pattern in Figs.5(a) – 5(d) do not reach this value. This is because that the beam fanning in our experiment is not a perfect thermal light, and the CCD detector is not a perfect detector due to the fact that CCD pixels can only register 256 grey values. Thus, we assume that $C_2 = 0.5$. The modification does not alter the main features of the interference patterns except for fringe magnitudes. By taking into account this modification, we obtain the theoretical simulation of the interference patterns indicated by the solid lines in Figs.5(a) – 5(d).

To better understand the physics behind the second-order interference for the thermal light, here we propose a simple theoretical description in terms of the Hanbury-Brown and Twiss effect.[23] We assume that a monochromatic beam of wavelength λ illuminates the double-slit, and the fields E_A and E_B at the two slits are completely incoherent, that is, the two fields are statistically independent

$$\langle E_A^* E_B \rangle = \langle E_A^* \rangle \langle E_B \rangle = 0, \tag{3}$$

where $\langle E_A \rangle = \langle E_B \rangle = 0$ is due to the random phase of the fields. As shown in Fig.6, P_1 and P_2 are two positions in the interference plane.

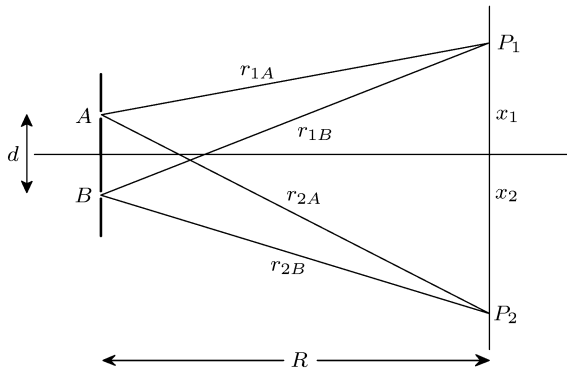


Fig.6. Sketch of the double-slit interference.

The amplitude and intensity at position P_i $(i = 1, 2)$ are obtained as

$$E(P_i) = (1/R)[E_A \exp(\mathrm{i}kr_{iA}) + E_B \exp(\mathrm{i}kr_{iB})], \qquad (i = 1, 2), \tag{4}$$

$$I(P_i) = (1/R^2)\left\{|E_A|^2 + |E_B|^2 + [E_A^* E_B \exp(\mathrm{i}kr_i) + \mathrm{c.c.}]\right\}, \qquad (i = 1, 2) \tag{5}$$

where $r_i \equiv r_{iB} - r_{iA}$ is the path difference from the two slits to position P_i. When the fields at the two slits are incoherent (i.e. Eq.(3)), it is well known that there is no first-order double-slit interference on the observation plane, so

$$\langle I(P_1) \rangle = \langle I(P_2) \rangle = (1/R^2)(\langle |E_A|^2 \rangle + \langle |E_B|^2 \rangle). \tag{6}$$

Then we consider the second-order double-slit interference by the joint-intensity measurement at two positions

$$\begin{aligned}\langle I(P_1) I(P_2) \rangle = (1/R^4)\Big\{ &\langle \left(|E_A|^2 + |E_B|^2\right)^2 \rangle + \left([\langle (E_A^*)^2 E_A E_B \rangle + \langle E_B^* (E_B)^2 E_A^* \rangle][e^{\mathrm{i}kr_1} + e^{\mathrm{i}kr_2}] + \mathrm{c.c.}\right) \\ &+ \left(\langle (E_A^*)^2 (E_B)^2 \rangle e^{\mathrm{i}k(r_1 + r_2)} + \mathrm{c.c.}\right) + \langle |E_A|^2 |E_B|^2 \rangle [e^{\mathrm{i}k(r_1 - r_2)} + \mathrm{c.c.}]\Big\}. \end{aligned} \tag{7}$$

Taking into account the incoherence of the fields at the two slits, we obtain

$$\begin{aligned}\langle I(P_1) I(P_2) \rangle &= (1/R^4)\left\{\langle |E_A|^4 \rangle + \langle |E_B|^4 \rangle + 2\langle |E_A|^2 \rangle \langle |E_B|^2 \rangle \left[1 + \cos k(r_1 - r_2)\right]\right\} \\ &= (1/R^4)\left\{\langle |E_A|^4 \rangle + \langle |E_B|^4 \rangle + 2\langle |E_A|^2 \rangle \langle |E_B|^2 \rangle \left[1 + \cos \frac{2\pi d}{\lambda R}(x_1 - x_2)\right]\right\}, \end{aligned} \tag{8}$$

where $x_i = r_i R/d$ is the transverse coordinate of position P_i. The first two terms introduce a background and the last term displays an interference pattern.

Equation (8) can explain all the experimental results above. If we scan the two detectors in the opposite direction around any position x_0, i.e. $x_1 = x + x_0$ and $x_2 = -x + x_0$, we observe the interference pattern $\left[1 + \cos\frac{2\pi d}{\lambda R} 2x\right]$, which shows a half fringe interval of that for the first-order interference. As for $x_1 = x$ and $x_2 = -nx$, we obtain the pattern $\left[1 + \cos\frac{2\pi d}{\lambda R}(n+1)x\right]$, which has been shown in Fig.5(c) for $n = 2$. If, however, one detector is scanned by fixing the other, the same interference pattern as the ordinary one $\left[1 + \cos\frac{2\pi d}{\lambda R}(x - x_0)\right]$ is observed. The second-order interference fringe disappears only when two detectors are scanned in the same direction, i.e. $x_1 = x$ and $x_2 = x_0 + x$.

The fringe visibility of the second-order interference can be defined and evaluated as

$$V \equiv \frac{\langle I(P_1)I(P_2)\rangle_{\max} - \langle I(P_1)I(P_2)\rangle_{\min}}{\langle I(P_1)I(P_2)\rangle_{\max} + \langle I(P_1)I(P_2)\rangle_{\min}} = \frac{2\langle|E_A|^2\rangle\langle|E_B|^2\rangle}{\langle|E_A|^4\rangle + \langle|E_B|^4\rangle + 2\langle|E_A|^2\rangle\langle|E_B|^2\rangle}. \quad (9)$$

If, for example, the fields at the two slits are random only in phase and their intensities are equal without fluctuation, i.e. $|E_A|^2 = |E_B|^2 = I_0$, the fringe visibility is 50%. However, if the source is thermal light satisfying ideal Gaussian statistics, it has $\langle|E|^4\rangle = 2\langle|E|^2\rangle^2$ and the visibility is 33.33%.

4. Conclusion

In summary, we have demonstrated experimentally the second-order double-slit interference with a new incoherent light source, the dynamic photorefractive beam fanning. The beam fanning produced in photorefractive crystal is not in a sense artificial such as the rotating ground glass, and it can act as a better thermal-like light source, possessing both a long correlation time and a wide spectral bandwidth, for performing the second-order interference and the correlated imaging. All the experimental results are in good agreement with the theoretical simulation according to the Hanbury-Brown and Twiss effect.

Acknowledgment

One of the authors, Wang Kaige, acknowledges the financial support of the Abdus Salam International Centre for Theoretical Physics (ICTP) under the Associate Programme.

References

[1] Wang K G and Cao D Z 2004 *Phys. Rev.* A **70** 041801(R)
[2] Cao D Z, Li Z, Zhai Y H and Wang K G 2005 *Eur. Phys. J.* D **33** 137
[3] Cao D Z and Wang K G 2004 *Phys. Lett.* A **333** 23
[4] Xiong J, Cao D Z, Huang F, Li H G, Sun X J and Wang K G 2005 *Phys. Rev. Lett.* **94** 173601
[5] Zhai Y H, Chen X H, Zhang D and Wu L A 2005 *Phys. Rev.* A **72** 043805
[6] D'Angelo M, Chekhova M V and Shih Y 2001 *Phys. Rev. Lett.* **87** 013602
[7] Gatti A, Brambilla E, Bache M and Lugiato L A 2004 *Phys. Rev. Lett.* **93** 093602
Gatti A, Brambilla E, Bache M and Lugiato L A 2004 *Phys. Rev.* A **70** 013802
[8] Cheng J and Han S 2004 *Phys. Rev. Lett.* **92** 093903
[9] Cai Y and Zhu S Y 2004 *Opt. Lett.* **29** 2716
[10] Bennink R S, Bentley S J and Boyd R W 2002 *Phys. Rev.Lett.* **89** 113601
Bennink R S, Bentley S J, Boyd R W and Howell J C 2004 *Phys. Rev. Lett.* **92** 033601
[11] Scarcelli G, Valencia A and Shih Y 2004 *Phys. Rev.* A **70** 051802(R)
[12] Magatti D, Ferri F, Gatti A, Bache M, Brambilla E and Lugiato L A 2005 *Phys. Rev. Lett.* **94** 183602
[13] Valencia A, Scarcelli G, D'Angelo M and Shih Y 2005 *Phys. Rev. Lett.* **94** 063601
[14] Zhang D, Zhai Y H, Wu L A and Chen X H 2005 *Opt. Lett.* **30** 2354
[15] Feinberg J 1982 *J. Opt. Soc. Am.* **72** 46
[16] Vally G C 1987 *J. Opt. Soc. Am.* B **4** 14
[17] Gu C and Yeh P 1991 *Opt. Lett.* **16** 1572
[18] Hong Y H, Xie P, Dai J H, Zhu Y, Yang H G and Zhang H J 1993 *Opt. Lett.* **18** 772
[19] Segev M, Engin D, Yariv A and Valley G C 1993 *Opt. Lett.* **18** 956
[20] Banerjee P P and Liu J J 1993 *J. Opt. Soc. Am.* B **10** 1417
[21] Zozulya A A and Anderson D Z 1995 *Phys. Rev.* A **52** 878
[22] Xiong J, Sun Y G and Hu G 2000 *Acta Opt. Sin.* **20** 145 (in Chinese)
[23] Hanbury-Brown R and Twiss R Q 1956 *Nature* **177** 27